Appl. Phys. B 77, 177–183 (2003)
DOI: 10.1007/s00340-003-1199-2

Applied Physics B
Lasers and Optics

N. AKÖZBEK[1,✉]
A. BECKER[2]
M. SCALORA[3]
S.L. CHIN[4]
C.M. BOWDEN[3]

Continuum generation of the third-harmonic pulse generated by an intense femtosecond IR laser pulse in air

[1] Time Domain Corporation, 7057 Old Madison Pike, Huntsville, AL, 35806, USA
[2] Max-Planck-Institut für Physik komplexer Systeme, Nöthnitzer Str. 38, 01187, Dresden, Germany
[3] U.S. Army Aviation and Missile Command, AMSAM-WS-RD-ST, Huntsville, AL 35898-5000, USA
[4] Département de Physique, de Génie Physique et d'Optique and Centre d'Optique, Photonique et Laser, Université Laval, Québec, Québec, G1K7P4, Canada

Received: 11 February 2003/Revised version: 23 April 2003
Published online: 6 June 2003 •

ABSTRACT The continuum generation by intense femtosecond IR laser pulses focused in air including the effect of third-harmonic generation is investigated. We have used a theoretical model that includes the full spatio-temporal dynamics of both the fundamental and the third-harmonic pulses. Results of our numerical calculations show that a two-color filamentation effect occurs, in which the third-harmonic conversion efficiency remains almost constant over the whole filament length. It is found that this effect is rather independent of the wavelength of the input beam and the focal geometry. During the filamentation process the third-harmonic pulse itself generates a broad continuum, which can even overlap with the continuum of the fundamental pulse for the longer pump wavelengths. In consequence, the continuum generation generated by intense IR laser pulses is further extended into the UV.

PACS 42.65.Jx; 42.65.Ky; 52.35.Mw

1 Introduction

Supercontinuum generation has been widely studied both experimentally and theoretically in the past [1, 2]. It is a universal phenomenon that has been observed both in gaseous [3–8] and condensed media [9–13]. The process of supercontinuum generation is quite complex; its main mechanism is related to self-phase modulation with additional contributions from stimulated Raman scattering, instantaneous electronic Kerr nonlinearity, temporal self-steepening, and four-photon parametric processes [14]. In general, the continuum generation depends on the input peak pulse power, the optical medium, and the focusing geometry.

In recent years there has been a growing interest in the propagation of intense femtosecond laser pulses in the atmosphere for possible applications in lidar measurements. It has been demonstrated both in the near IR [6, 7, 15–18] and the UV [19, 20] that long self-induced filaments are generated when sub-picosecond high-peak-power laser pulses are propagated in air. The supercontinuum generated during the filamentation process has been used for time-resolved broadband spectroscopy [6, 7]. The filamentation process depends mainly on two competing processes. At first, the spatial intensity profile of the laser pulse acts like a focusing lens due to the optical Kerr effect. This causes the beam to self-focus, resulting in an increase of the peak intensity. At high peak intensity multiphoton ionization of the medium sets in and creates a low-density plasma. Since the refractive index of the plasma is lower than that of neutral air, the beam defocuses again. The competition between defocusing and self-focusing (and several smaller nonlinear effects) finally gets balanced in a quasi-equilibrium and a stable filament is created. The details of the dynamics of the filamentation process are complex and different interpretations such as the moving focus picture [17], the self-channeling model [15, 16, 18], or spatial replenishment [21] have been proposed.

Although the peak intensity in the filaments is found to be clamped down to about 10^{13} W/cm^2 [22–24], it is sufficient to generate efficient higher harmonics [22, 25–30]. Recently, we have shown [31] that the third-harmonic pulse indeed copropagates together with the fundamental pulse over the whole length of the filament with a constant-envelope phase difference. During the cofilamentation process the third-harmonic pulse maintains both its peak intensity and energy over distances much longer than the characteristic coherence length. This is in contrast to harmonic generation in bulk media, where a certain phase relation between fundamental and harmonic pulses can be maintained over a limited nonlinear interaction length only. The strong interaction and an effective nonlinear phase-locking mechanism between the pump and the third-harmonic pulses lead to what we refer to as two-color filamentation.

One of the important consequences of the two-color filamentation is a strong cross-phase modulation and a spectral broadening of the third-harmonic pulse. In this theoretical study we show that the third-harmonic pulse is expected to undergo continuum generation together with the pump pulse. As a result, the efficient third-harmonic generation inside the filament should potentially extend the white-light spectrum into the UV. This is important since it has been observed before [24] that the lower extent of the continuum generation of the pump pulse is limited to about 350 nm in air. A similar limitation of the supercontinuum spectrum in condensed matter has been recently attributed to the clamping of the peak intensity inside the filaments [32]. It is therefore of much interest to investigate the generation of the supercontinuum spectrum of

✉ Fax: +1-256/955-7216, E-mail: neset.akozbek@timedomain.com

a femtosecond laser pulse in air including the effect of third-harmonic generation.

To this end, we examine below third-harmonic generation and filamentation in air under various input conditions using different input pump wavelengths and focal geometries. We consider pump wavelengths at 800, 1064, and 1550 nm. Ti:sapphire laser systems operating at 800 nm can produce peak powers in the terawatt region, and recently femtosecond terawatt laser systems at 1.06 micron have been demonstrated [33]. The wavelength 1550 nm is particularly important for lidar types of applications where it may be required to use eye-safe lasers. The outline of the paper is as follows: in Sect. 2 we present the theoretical model used to study the propagation of a fundamental laser pulse together with the generation and propagation of its third harmonic. In Sect. 3 results of the numerical calculations for the on-axis peak intensity of the fundamental and the third-harmonic conversion efficiency for different input laser conditions will be presented and discussed in view of the universality of the co-filamentation phenomenon. Section 4 provides the central result of this article, namely the continuum generation of both fundamental and third-harmonic pulses.

2 Theory

In order to study the dynamics of third-harmonic generation by an intense ultra-short laser pulse during filamentation in gases it is necessary to include the full spatio-temporal dynamics of both the fundamental and the third-harmonic pulses. Our model is described by a set of coupled equations, which can be written in dimensionless form in the retarded coordinate system ($\tau = t - z/v_g(\omega)$) as [31, 34, 35]:

$$\left(\mathrm{i}\frac{\partial}{\partial z}+\frac{1}{4}\nabla_\perp^2-\mathrm{i}\frac{L_{\mathrm{DF}}}{4L_{\mathrm{d}}}\frac{\partial^2}{\partial\tau^2}+\mathrm{i}\frac{L_{\mathrm{DF}}}{L_{\mathrm{Abs}}}\left|\mathcal{E}_\omega\right|^{2n-2}\right)\mathcal{E}_\omega + \frac{L_{\mathrm{DF}}}{L_{\mathrm{NL}}}\left(\left|\mathcal{E}_\omega\right|^2\mathcal{E}_\omega+\mathcal{E}_\omega^{*2}\mathcal{E}_{3\omega}+2\left|\mathcal{E}_{3\omega}\right|^2\mathcal{E}_\omega\right)-\frac{L_{\mathrm{DF}}}{L_{\mathrm{PL}}}N_{\mathrm{e}}\mathcal{E}_\omega=0\,, \tag{1}$$

$$\left(\mathrm{i}\frac{\partial}{\partial z}+\frac{1}{12}\nabla_\perp^2+\mathrm{i}\frac{L_{\mathrm{DF}}}{L_{\Delta v}}\frac{\partial}{\partial\tau}-\mathrm{i}\frac{L_{\mathrm{DF}}}{4L_{\mathrm{d}}'}\frac{\partial^2}{\partial\tau^2}+\frac{L_{\mathrm{DF}}}{L_{\Delta k}}\right)\mathcal{E}_\omega - \frac{L_{\mathrm{DF}}}{3L_{\mathrm{PL}}}N_{\mathrm{e}}\mathcal{E}_{3\omega}+\mathrm{i}\frac{L_{\mathrm{DF}}}{L_{\mathrm{Abs}}}\left|\mathcal{E}_{3\omega}\right|^{2n-2}\mathcal{E}_{3\omega} + \frac{3L_{\mathrm{DF}}}{L_{\mathrm{NL}}}\left(\left|\mathcal{E}_{3\omega}\right|^2\mathcal{E}_{3\omega}+\frac{\mathcal{E}_\omega^3}{3}+2\left|\mathcal{E}_\omega\right|^2\mathcal{E}_{3\omega}\right)=0\,, \tag{2}$$

$$\frac{\partial N_{\mathrm{e}}(\tau)}{\partial\tau}=(\Gamma_\omega+\Gamma_{3\omega})\left(1-N_{\mathrm{e}}(\tau)\right). \tag{3}$$

Here, $\mathcal{E}_\omega$ and $\mathcal{E}_{3\omega}$ are the electric field envelope functions, normalized to the peak value of the input pump field $\mathcal{E}_0=\sqrt{2P_0/\pi w_0^2}$; the transformation $\mathcal{E}_{3\omega}\to\mathcal{E}_{3\omega}\mathrm{e}^{\mathrm{i}\Delta kz}$ was also used. The sub- and superscripts, ω and 3ω, denote the fundamental and third-harmonic pulses, respectively. The propagation direction z is given in units of $L_{\mathrm{DF}}=k_\omega w_0^2/2$, the temporal coordinate τ in units of the input pulse width τ_0, and the transverse coordinate r in units of the input beam radius w_0. The following length scales are also used: $L_{\mathrm{NL}}=(n_2k_\omega I_0)^{-1}$ is a nonlinear length

λ_0 (nm)	Δk (cm^{-1})	Δv (cm/s)	k''_ω (fs^2/cm)	$k''_{3\omega}$ (fs^2/cm)	P_{cr} (GW)
800	−5.0	0.4	0.20	1.00	3
1064	−3.0	0.6	0.16	0.75	6
1550	−0.65	2.0	0.10	0.35	10

TABLE 1 Parameters used for each pump wavelength

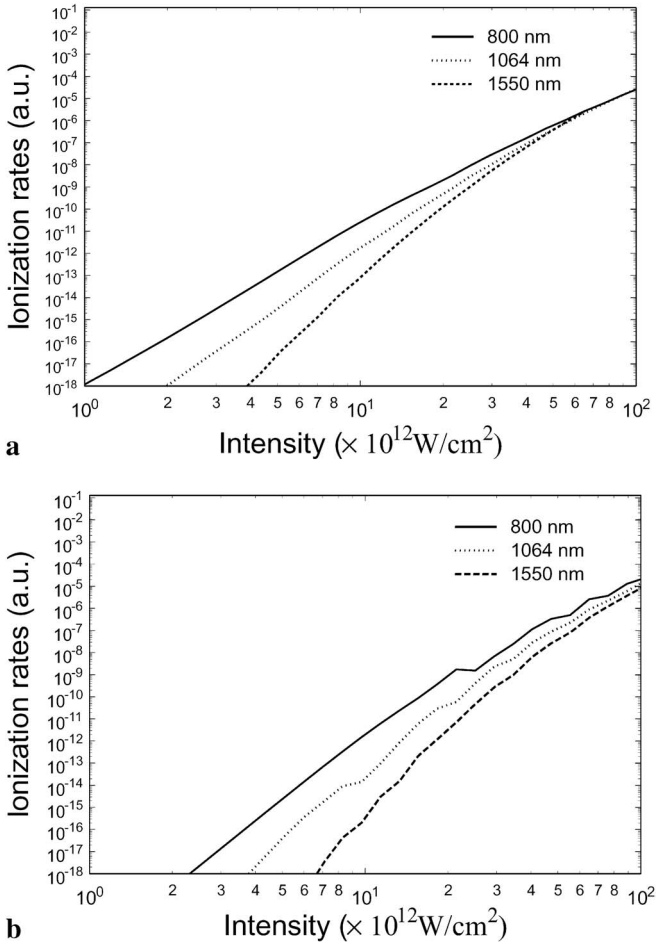

FIGURE 1 Ionization rates of **a** O_2 and **b** N_2 as a function of the laser intensity at the three laser wavelengths, 800 nm (*solid lines*), 1064 nm (*dotted lines*), and 1550 nm (*dashed lines*), as calculated by a theoretical model for ionization of molecules in strong fields

λ (nm)	800	1064	1550	267	310	520
σ_{O_2} (s^{-1})	1.8×10^{-83}	3.4×10^{-107}	8.5×10^{-150}	1.5×10^{-14}	2.4×10^{-28}	9.0×10^{-55}
n_{O_2}	6.8	8.5	11.6	1.9	2.9	4.7
σ_{N_2} (s^{-1})	4×10^{-110}	8.5×10^{-136}	4.4×10^{-181}	3.6×10^{-29}	7.2×10^{-32}	9.0×10^{-73}
n_{N_2}	8.7	10.5	13.8	3.0	3.2	6.1

TABLE 2 Fitting parameters σ and n for the ionization rates shown in Fig. 1

scale, where $I_0 = |\mathcal{E}_0|^2$ and $n_2 = 4 \times 10^{-19}\,\mathrm{cm}^2/\mathrm{W}$, and $L_{\mathrm{PL}} = k_\omega m_e c^2/2\pi e^2 N_0$ is the plasma length scale, where N_0 is the number density of neutral air molecules. $L_{\Delta v} = \Delta v \tau_0$, where $1/\Delta v = v_g^{-1}(3\omega) - v_g^{-1}(\omega)$, represents the characteristic temporal walk-off distance due to the group-velocity mismatch between the fundamental and third-harmonic pulses. $L_d = \tau_0^2/2k''_\omega$ and $L'_d = \tau_0^2/2k''_{3\omega}$ are the length scales due to group-velocity dispersion of the fundamental and third harmonic, respectively. Finally, $L_{\Delta k} = |\Delta k|^{-1} = |3k_\omega - k_{3\omega}|^{-1}$ is the linear wavevector mismatch length scale in the wavevectors $k_\omega = n_\omega k_0$ and $k_{3\omega} = n_{3\omega} 3k_0$, where $\Delta k = 3k_0\,(n_\omega - n_{3\omega})$. All the relevant parameters used in the calculations for each wavelength are listed in Table 1.

Electron generation through multiphoton ionization of N_2 and O_2 is taken into account by the rates Γ_ω and $\Gamma_{3\omega}$. In the course of the numerical calculations, it has been found that, in general, the influence of ionization and plasma generation by the third harmonic on the results presented below is small. The rates are calculated using a rate formula, developed for multiphoton ionization of di- and polyatomic molecules in strong laser fields [36, 37]. This model has been tested well before [36] against experimental ion yields of N_2 and O_2 at the Ti:sapphire laser wavelength. In Fig. 1 we present the rates for ionization of O_2 (panel a) and N_2 (panel b) as a function of the laser intensity at the three wavelengths 800 nm (solid lines), 1064 nm (dotted lines), and 1550 nm (dashed lines), which we have considered for the pump laser in our simulations. In all cases the rates follow rather straight lines in the log–log plots of Fig. 1, which suggests further approximating the rates by a fit to the form $\Gamma = \sigma I^n$ for the relevant intensity range up to about $10^{14}\,\mathrm{W/cm}^2$. The same is found to hold for the rates at the third-harmonic wavelengths. In Table 2 the parameters σ and n used in the present numerical calculations are given. Note that the exponents n are not integer numbers. This indicates that the interaction between the intense laser field and the molecules is nonperturbative. The rates are also found to depend on the laser wavelength below $10^{14}\,\mathrm{W/cm}^2$. Thus, tunnel ionization theory, such as the well-known ADK formula [38], is not applicable. The wavelength and intensity regime of present interest is therefore characterized best as the nonperturbative multiphoton regime.

3 Third-harmonic generation and self-channeling

We have considered the propagation of linearly polarized, collimated Gaussian input laser pulses at three different center wavelengths, namely $\lambda_0 = 800\,\mathrm{nm}$, 1064 nm, and 1550 nm, having a beam radius of $w_0 = 0.5\,\mathrm{cm}$ $(1/\mathrm{e}^2)$

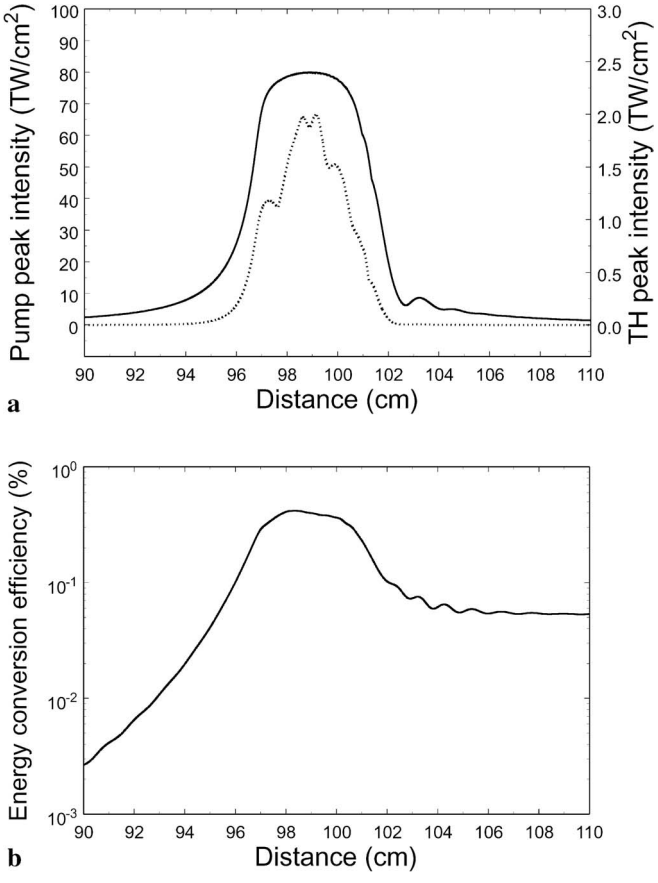

FIGURE 2 Results of numerical calculations for **a** the on-axis peak intensities of the fundamental pulse (*solid line*) and the third-harmonic pulse (*dotted line*) and **b** the third-harmonic conversion efficiency as a function of the propagation distance for a focal length of $f = 100\,\mathrm{cm}$. The laser parameters of the input beam were $\lambda_0 = 800\,\mathrm{nm}$, $w_0 = 0.5\,\mathrm{cm}$ $(1/e^2)$, $\tau_{\mathrm{FWHM}} = 50\,\mathrm{fs}$, and $P_0 = 3.0 P_{\mathrm{cr}}$

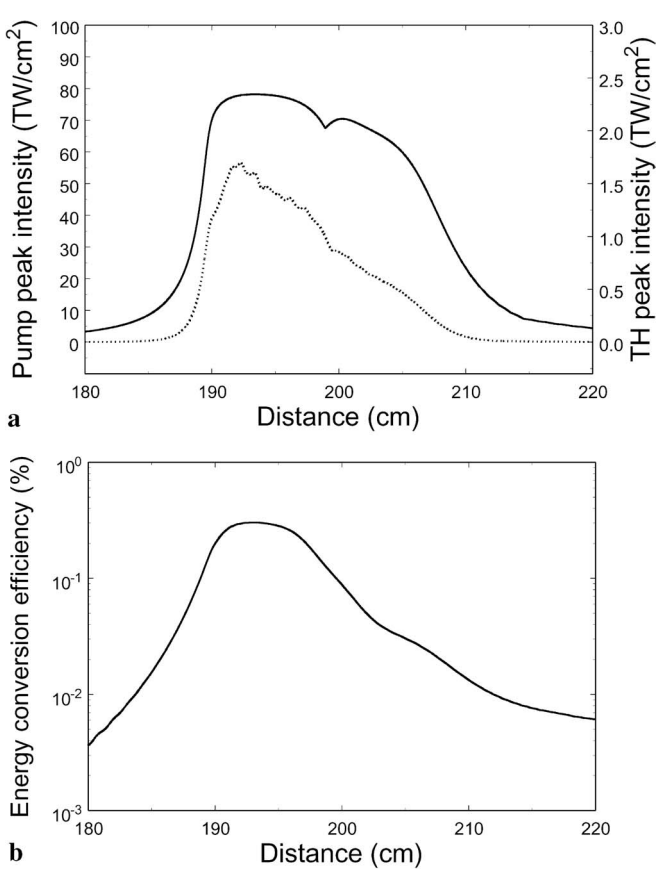

FIGURE 3 Results of numerical calculations for **a** the on-axis peak intensity of the fundamental pulse (*solid line*) and the third-harmonic pulse (*dotted line*) and **b** the third-harmonic conversion efficiency as a function of the propagation distance for a focal length of $f = 200\,\mathrm{cm}$. The laser parameters of the input beam were $\lambda_0 = 800\,\mathrm{nm}$, $w_0 = 0.5\,\mathrm{cm}$ $(1/e^2)$, $\tau_{\mathrm{FWHM}} = 50\,\mathrm{fs}$, and $P_0 = 3.0 P_{\mathrm{cr}}$

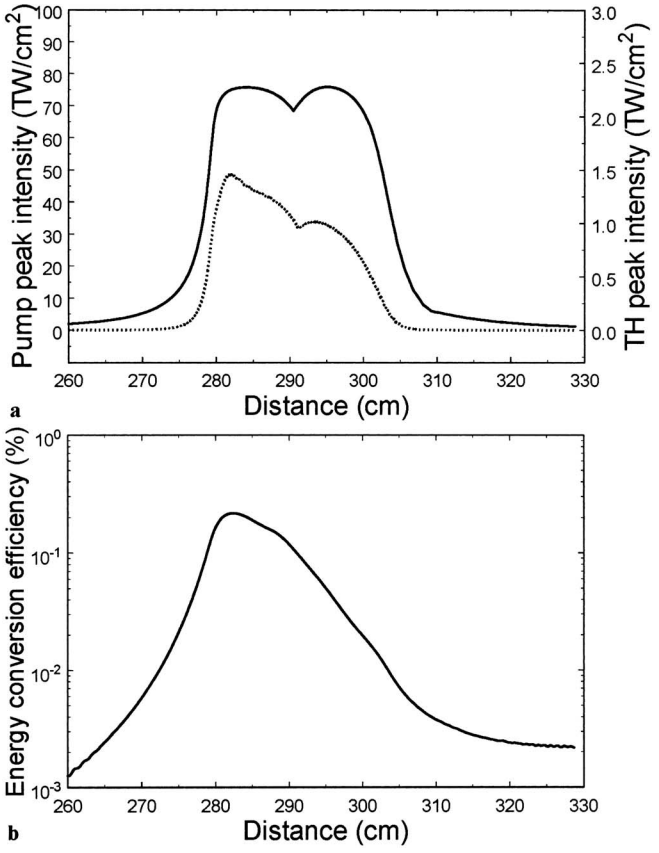

FIGURE 4 Results of numerical calculations for **a** the on-axis peak intensity of the fundamental pulse (*solid line*) and the third-harmonic pulse (*dotted line*) and **b** the third-harmonic conversion efficiency as a function of the propagation distance for a focal length of $f = 300$ cm. The laser parameters of the input beam were $\lambda_0 = 800$ nm, $w_0 = 0.5$ cm $(1/e^2)$, $\tau_{\mathrm{FWHM}} = 50$ fs, and $P_0 = 3.0 P_{\mathrm{cr}}$

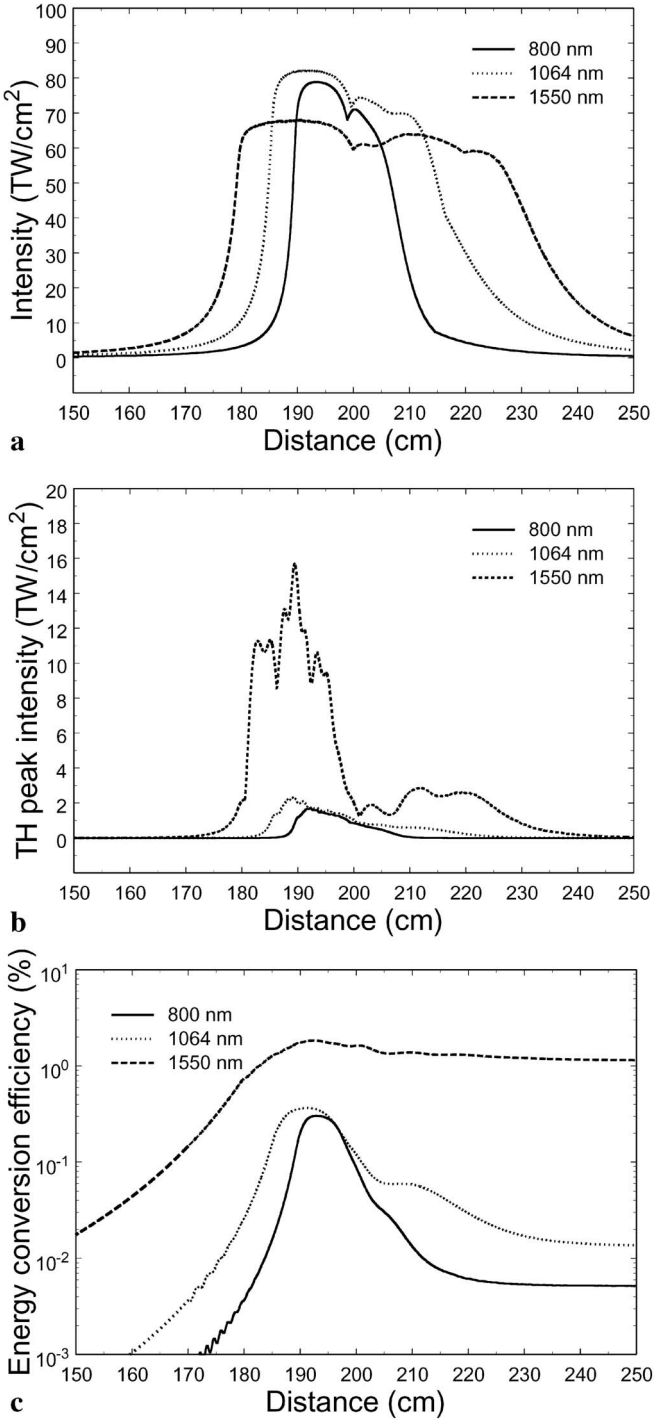

FIGURE 5 Results of numerical calculations for **a** the on-axis peak intensity of the fundamental pulse, **b** the on-axis peak intensity of the third-harmonic pulse, and **c** the third-harmonic conversion efficiency as a function of the propagation distance (normalized to the geometrical focal point). A comparison is shown for three wavelengths, 800 nm (*solid lines*), 1064 nm (*dotted lines*), and 1550 nm (*dashed lines*). The focal length was $f = 200$ cm and the other laser parameters were the same as in Fig. 2

and a pulse duration of $\tau_{\mathrm{FWHM}} = 50$ fs, which are typical for current high-peak-power femtosecond laser sources. The initially collimated beam is assumed to be focused in air at atmospheric pressure by an external lens with focal lengths of $f = 100$ cm, 200 cm, and 300 cm, respectively. Since we are primarily interested in third-harmonic generation under filament formation, we have used laser input powers above the critical power, $P_{\mathrm{cr}} = \lambda_0^2/2\pi n_\omega n_2$ (see Table 1), needed for self-focusing and filamentation. The set of equations (1)–(3) is integrated numerically with the initial condition $\mathcal{E}_{3\omega}(z = 0) = 0$.

First, we present and discuss the results for laser pulse filamentation at the wavelength of the widely used Ti:sapphire laser system, namely 800 nm. In Fig. 2a the pump (solid line, left scale) and third harmonic (dotted line, right scale) on-axis peak intensities and in Fig. 2b the third-harmonic conversion efficiency are plotted as a function of propagation distance for a focal length of $f = 100$ cm. Due to the self-focusing effect the pulse comes to focus before the geometrical focal point and maintains its high peak intensity over several centimeters (Fig. 2a, solid line). This provides a long nonlinear interaction length, which otherwise is limited to the confocal length when input powers below critical powers are used. As a result, the third-harmonic pulse channels together with the fundamental pulse (Fig. 2a, dotted line). It is important to note that the length of the filament is a distance of many coherence lengths. This phenomenon of two-color filamentation has been confirmed by us in a recent experiment and attributed as due to a nonlinear phase-locking mechanism [31]. The effect qualitatively does not depend on the focal geometry; results for $f = 200$ cm and $f = 300$ cm are shown in Figs. 3 and 4, re-

spectively. In all cases the conversion efficiency is high over the entire filament length, as can be seen in Figs. 2b, 3b, and 4b. We, however, observe that the conversion efficiency drops more strongly towards the end of the filament the longer is the focal length. The maximum conversion efficiency is found to depend weakly on the focal length, reaching the highest value of 0.5% for the shortest focal length $f = 100$ cm.

In order to show that this phenomenon does not depend on the particular choice of beam parameters, we have also studied filamentation and third-harmonic generation at pump wavelengths of 1064 nm and 1550 nm. In Fig. 5 we show a comparison of the pump peak intensity (panel a), the third-harmonic peak intensity (panel b), and the third-harmonic conversion efficiency (panel c) at the three wavelengths (800 nm: solid lines, 1064 nm: dotted lines, 1550 nm: dashed lines) using a focal length $f = 200$ cm. An important observation is that the clamped peak intensity inside the filament is about 10^{13} W/cm^2, in agreement with recent experimental observations [22, 23] and theoretical estimations [24]. The clamped peak intensity is found to be almost the same for all wavelengths despite the fact that more photons are required to ionize the air molecules at 1064 nm and 1550 nm. This, however, can be understood from the ionization rates at the three wavelengths, which are getting close to each other in this intensity regime (cf. Fig. 1). As can be seen from Fig. 5b, the qualitative aspect of the co-propagation of the fundamental and the third-harmonic pulses together in the filament is also independent of the input laser wavelength. But, there are significant differences in the third-harmonic conversion efficiency for the different wavelengths. It is apparent that the conversion efficiency at 1550 nm (Fig. 5c, dashed line) is nearly an order of magnitude higher than at 800 nm (Fig. 5c, solid line), even though the peak pump intensity at 1550 nm is slightly lower (cf. Fig. 5a). This indicates that the initial wavevector mismatch between the pump and the third-harmonic pulses, which is considerably smaller at 1550 nm than it is at 800 nm or 1064 nm, is an important parameter for the co-propagation process and the conversion of pump-pulse energy into third-harmonic pulse energy.

The strong interaction between the pump and the third-harmonic pulses over a long interaction length leads to a rich spatio-temporal dynamics of the two pulses. To demonstrate this, in Fig. 6 we plot the spatio-temporal intensity distribution of both the pump and third-harmonic pulses in the case of 800-nm pump wavelength and $f = 200$ cm at two different propagation positions. It is evident that the third-harmonic pulse exhibits similar features as the pump pulse, namely self-focusing (Fig. 6a) and temporal pulse splitting (Fig. 6b). This close correlation in the spatio-temporal dynamics of both the pulses is not surprising, since the third-harmonic pulse is generated by the strong pump pulse.

4 Third-harmonic-pulse continuum generation

The close correlation of the pump and third-harmonic pulses should induce a strong cross-phase modu-

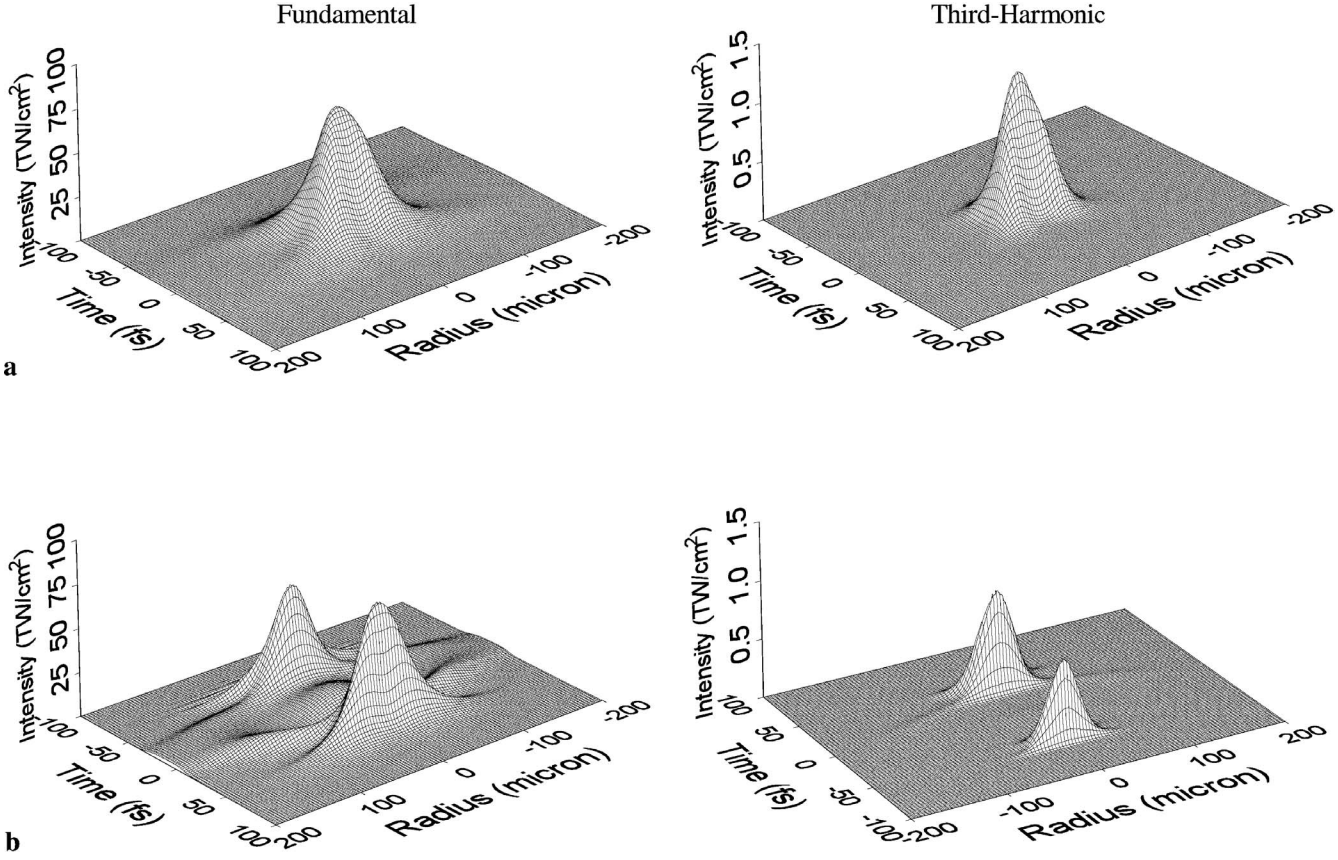

FIGURE 6 Numerical results for the spatio-temporal intensity distribution of the fundamental pulse (*left*) and third-harmonic pulse (*right*) at **a** $z = 190$ cm and **b** $z = 200$ cm. A focal length of 200 cm and laser parameters as in Fig. 2 were chosen

lation, which should manifest itself by a spectral broadening of the third-harmonic pulse. This is indeed what we observe for each of the three pump laser wavelengths. In Fig. 7 we show the supercontinuum generated by both the fundamental and the third-harmonic pulses, at (a) 800 nm, (b) 1064 nm, and (c) 1550 nm, at a propagation $z = 200$ cm (a focal length of $f = 200$ cm was chosen). For the sake of comparison we have also plotted by dotted lines the respective fundamental pulse and the third-harmonic pulse just before the filamentation process starts. The comparison reveals that both the pulses are getting broadened during the filamentation process. In view of our interest in the propagation dynamics of the third-harmonic pulse, we find for the present beam parameters and focal geometry third-harmonic continua ranging from 250 nm to 350 nm (Fig. 7a, $\lambda_0 = 800$ nm), from 280 nm to 580 nm (Fig. 7b, $\lambda_0 = 1064$ nm), and from 350 nm to 800 nm (Fig. 7c, $\lambda_0 = 1550$ nm).

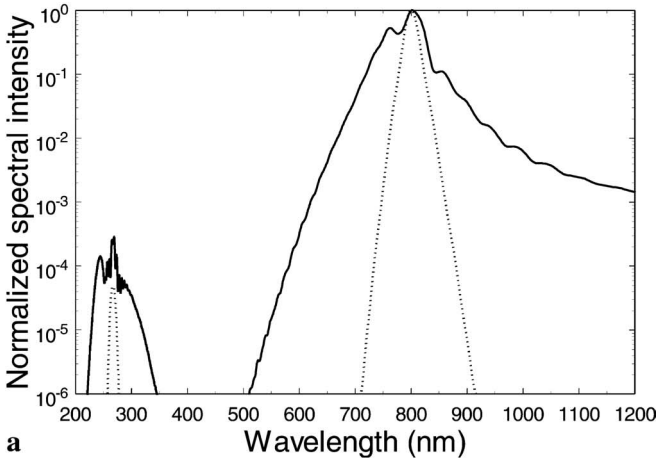

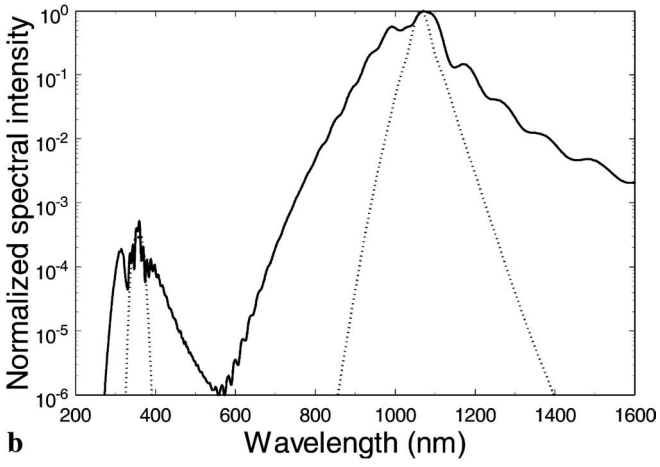

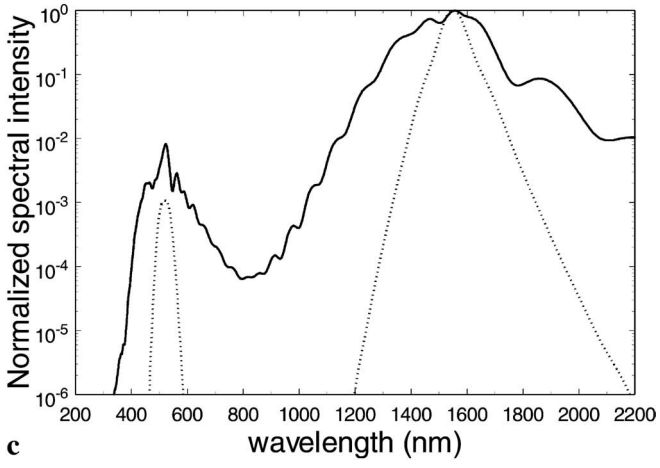

FIGURE 7 Spectrum of the fundamental and the third-harmonic pulses before filamentation (*dotted lines*) and in the filament (at $z = 200$ cm, *solid lines*) are compared for three wavelengths of the pump laser, **a** 800 nm, **b** 1064 nm, and **c** 1550 nm

For all three wavelengths the two continua, due to the fundamental and due to the third harmonic, are essentially separated with a minimum in between. This minimum is strongest for the shortest wavelength, i.e. 800 nm, where the two continua are found to be clearly separated (at these beam parameters and the present focal geometry). On the other hand, at 1550 nm, the minimum is rather weak and we may describe the whole spectrum as a supercontinuum extending from about 400 nm up to far above 2200 nm.

Continuum generation of a harmonic was shown previously [39] in the case of second-harmonic generation in condensed matter and was attributed to cross-phase modulation by the pump pulse. We find this to be the case here as well. In order to confirm it, we have propagated a pulse at 267 nm (i.e. the third harmonic of a pump pulse at 800 nm) alone under similar conditions; the spectrum did not show any signature of continuum generation. This is due to the fact that in air the clamped peak intensity inside the filament of a UV pulse is much lower than the corresponding intensity in the filaments of an IR pulse. Consequently, the intensities during UV pulse filamentation are not high enough to cause strong self-phase modulation of the pulse. Thus, the spectral broadening of the third harmonic, generated by the IR laser pulse, is mainly due to cross-phase modulation induced by the pump pulse rather than self-phase modulation of the third harmonic.

5 Conclusions and outlook

In conclusion, we have investigated the generation of a strong third-harmonic pulse during the propagation and filamentation of an ultra-short high-power laser pulse that is focused in air. Results of our numerical calculations show that a high conversion efficiency is maintained over the whole length of the filament, which is a distance much longer than the characteristic coherence length. Variations of the pump laser wavelength and the focal length indicate that the co-filamentation effect is rather independent of the input parameters; however, the strength of the conversion efficiency is found to depend on the wavelength.

The strong interaction between the fundamental and the third-harmonic pulses does not only lead to a rich spatio-temporal dynamics of the third-harmonic pulse, but, more important, to a continuum generation of the third-harmonic pulse itself. The continuum spectrum of the third harmonic can extend over several hundreds of nm and may even overlap with the continuum spectrum generated by the fundamental pulse, depending on the initial pump laser wavelength. The broadening of the third harmonic is found to be rather due to

a cross-phase modulation between the two pulses than due to a self-phase modulation of the third-harmonic pulse itself.

The continuum spectrum of the third-harmonic pulse offers important possible applications in laser pulse propagation in the atmosphere. It has been observed that the lower extent of the continuum spectrum is limited to about 350 nm in air. The results, shown in the present article, indicate that it should be possible to create a strong third harmonic and a corresponding continuum spectrum at remote distances. This might extend the effective spectral region of atmospheric sensing methods further in the UV and, hence, into an important wavelength regime for monitoring chemical pollutants and biological species.

ACKNOWLEDGEMENTS This work has been supported in part by NSERC, DREV, le Fonds FCAR, CIPI, and Canada Research Chairs. N.A. was supported by the US Army Research Office under Contract No. DAAD 19-02-C-0091.

REFERENCES

1 R.R. Alfano (Ed.): *The Supercontinuum Laser Source* (Springer, New York 1989)
2 S.L. Chin, A. Brodeur, S. Petit, O.G. Kosareva, V.P. Kandidov: J. Nonlinear Opt. Phys. Mater. **8**, 121 (1999)
3 P.B. Corkum, C. Rolland, T. Srinivasan-Rao: Phys. Rev. Lett. **57**, 2268 (1986)
4 H. Nishioka, W. Odajima, K. Ueda, H. Takuma: Opt. Lett. **20**, 2505 (1995)
5 E.T.J. Nibbering, M. Franco, B.S. Prade, G. Grillon, C. LeBlanc, A. Mysyrowicz: Opt. Commun. **119**, 479 (1995)
6 L. Wöste, C. Wedekind, H. Wille, P. Rairoux, B. Stein, S. Nikolov, C. Werner, S. Niedermeier, F. Ronneberger, H. Schillinger, R. Sauerbrey: Laser Optoelektronik **29**, 51 (1997)
7 P. Rairoux, H. Schillinger, S. Niedermeier, M. Rodriguez, F. Ronneberger, R. Sauerbrey, B. Stein, D. Waite, C. Wedekind, H. Wille, L. Wöste, C. Ziener: Appl. Phys. B **71**, 573 (2000)
8 J. Kasparian, R. Sauerbrey, D. Mondelain, S. Niedermeier, J. Yu, J.-P. Wolf, Y.-B. Andre, M. Franco, B. Prade, S. Tzortzakis, A. Mysyrowicz, M. Rodriguez, H. Wille, L. Wöste: Opt. Lett. **25**, 1397 (2000)
9 W.J. Jones, B.P. Stoicheff: Phys. Rev. Lett. **13**, 657 (1964)
10 N. Bloembergen, P. Lallemend: Phys. Rev. Lett. **16**, 81 (1966)
11 F. Shimizu: Phys. Rev. Lett. **19**, 1097 (1967)
12 A. Brodeur, S.L. Chin: Phys. Rev. Lett. **80**, 4406 (1998)
13 A. Brodeur, S.L. Chin: J. Opt. Soc. Am. B **16**, 637 (1999)
14 For a discussion of the main influences on the process of supercontinuum generation, see e.g. V.P. Kandidov, O.G. Kosareva, I.S. Golubtsov, W. Liu, A. Becker, N. Aközbek, C.M. Bowden, S.L. Chin: Appl. Phys. B (2003), DOI 10.1007/s00340-003-1214-7
15 A. Braun, G. Korn, X. Liu, D. Du, J. Squier, G. Mourou: Opt. Lett. **20**, 73 (1995)
16 E.T.J. Nibbering, P.F. Curley, G. Grillon, B.S. Prade, M.A. Franco, F. Salin, A. Mysyrowicz: Opt. Lett. **21**, 62 (1996)
17 A. Brodeur, C.Y. Chien, F.A. Ilkov, S.L. Chin, O.G. Kosareva, V.P. Kandidov: Opt. Lett. **22**, 304 (1997)
18 H.R. Lange, G. Grillon, J.F. Ripoche, M.A. Franco, B. Lamoroux, B.S. Prade, A. Mysyrowicz: Opt. Lett. **23**, 120 (1998)
19 J. Schwarz, P. Rambo, J.-C. Diels, M. Kolesik, E.M. Wright, J.V. Moloney: Opt. Commun. **180**, 383 (2000)
20 S. Tzortzakis, B. Lamouroux, A. Chiron, M. Franco, B. Prade, A. Mysyrowicz, D.S. Moustaizis: Opt. Lett. **25**, 1270 (2000)
21 M. Mlejnek, E.M. Wright, J.V. Moloney: Opt. Lett. **23**, 382 (1998)
22 H.R. Lange, A. Chiron, J.-F. Ripoche, A. Mysyrowicz, P. Breger, P. Agostini: Phys. Rev. Lett. **81**, 1611 (1998)
23 A. Becker, N. Aközbek, K. Vijayalakshmi, E. Oral, C.M. Bowden, S.L. Chin: Appl. Phys. B **73**, 287 (2001)
24 J. Kasparian, R. Sauerbrey, S.L. Chin: Appl. Phys. B **71**, 877 (2000)
25 S. Bachus, J. Peatross, Z. Zeek, A. Rundquist, G. Taft, M.M. Murnane, H.C. Kapteyn: Opt. Lett. **21**, 665 (1996)
26 C.W. Siders, N.C. Turner III, M.C. Downer, A. Babine, A. Stepanov, A.M. Sergeev: J. Opt. Soc. Am. B **13**, 330 (1996)
27 A.B. Fedotov, N.I. Koroteev, M.M.T. Loy, X. Xiao, A.M. Zheltikov: Opt. Commun. **133**, 587 (1997)
28 Y. Tamaki, J. Itatani, Y. Nagata, M. Obara, K. Midorikawa: Phys. Rev. Lett. **82**, 1422 (1999)
29 G. Marcus, A. Zigler, Z. Henis: J. Opt. Soc. Am. B **16**, 792 (1999)
30 Zhu Chang-jun, Qin Yuan-dong, Yang Hong, Wang Shu-feng, Gong Qihuang: Chin. Phys. Lett. **18**, 57 (2001)
31 N. Aközbek, A. Iwasaki, A. Becker, M. Scalora, S.L. Chin, C.M. Bowden: Phys. Rev. Lett. **89**, 143 901 (2002)
32 W. Liu, S. Petit, A. Becker, N. Aközbek, C.M. Bowden, S.L. Chin: Opt. Commun. **202**, 189 (2002)
33 Z. Xu, X. Yang, Y. Leng, H. Lu, L. Lin, Z. Zhang, R. Li, W. Zhang, D. Yin, S. Jin, J. Peng, B. Tang, B. Zhao: Chin. Opt. Lett. **1**, 24 (2003)
34 N. Aközbek, C.M. Bowden, A. Talebpour, S.L. Chin: Phys. Rev. E **61**, 4540 (2000)
35 N. Aközbek, C.M. Bowden, S.L. Chin: Opt. Commun. **191**, 353 (2001)
36 J. Muth-Böhm, A. Becker, F.H.M. Faisal: Phys. Rev. Lett. **85**, 2280 (2000)
37 J. Muth-Böhm, A. Becker, S.L. Chin, F.H.M. Faisal: Chem. Phys. Lett. **337**, 313 (2001)
38 M.V. Ammosov, N.B. Delone, V.P. Krainov: Zh. Eksp. Teor. Fiz. **91**, 2008 (1986) [Sov. Phys. JETP **54**, 1191 (1986)]
39 R.R. Alfano, Q.Z. Wang, T. Jimbo, P.P. Ho, R.N. Bhargava, B.J. Fitzpatrick: Phys. Rev. A **35**, 459(R) (1987)